HHS Public Access

Author manuscript

Sci Transl Med. Author manuscript; available in PMC 2016 December 16.

Published in final edited form as:

Sci Transl Med. 2015 December 16; 7(318): 318ra203. doi:10.1126/scitranslmed.aac4877.

Improving the spatial resolution of epiretinal implants by increasing stimulus pulse duration

Andrew C. Weitz[1,2], **Devyani Nanduri**[1], **Matthew R. Behrend**[3], **Alejandra Gonzalez-Calle**[1], **Robert J. Greenberg**[4], **Mark S. Humayun**[1,2], **Robert H. Chow**[1,5,*], and **James D. Weiland**[1,2,3]

[1]Department of Biomedical Engineering, Viterbi School of Engineering, University of Southern California, Los Angeles, CA 90089, USA

[2]Department of Ophthalmology, Keck School of Medicine, University of Southern California, Los Angeles, CA 90033, USA

[3]Department of Electrical Engineering, Viterbi School of Engineering, University of Southern California, Los Angeles, CA 90089, USA

[4]Second Sight Medical Products, Inc., Sylmar, CA 91342, USA

[5]Department of Physiology & Biophysics, Keck School of Medicine, University of Southern California, Los Angeles, CA 90033, USA

Abstract

Retinal prosthetic implants are the only approved treatment for retinitis pigmentosa, a disease of the eye that causes blindness through gradual degeneration of photoreceptors. An array of microelectrodes triggered by input from a camera stimulates surviving retinal neurons, each electrode acting as a pixel. Unintended stimulation of retinal ganglion cell axons causes patients to see large, oblong shapes of light, rather than focal spots, making it difficult for them to perceive forms. To address this problem, we performed calcium imaging in isolated retinas and mapped the patterns of cells activated by different electrical stimulation protocols. We found that pulse durations two orders of magnitude longer than those typically used in existing implants stimulate inner retinal neurons while avoiding activation of ganglion cell axons, thus confining retinal responses to the site of the electrode. We show that multielectrode stimulation with 25-ms pulses can pattern letters on the retina corresponding to a Snellen acuity of 20/312. We validated our findings in a patient with an implanted epiretinal prosthesis by demonstrating that 25-ms pulses evoke focal spots of light.

[*]Corresponding authors. jweiland@med.usc.edu or rchow@med.usc.edu.

Author contributions: A.C.W. conducted the animal experiments. D.N. conducted the human patient testing. M.R.B. developed many of the experimental methods. A.G.C. conducted the electrochemical measurements. A.C.W., D.N., and J.D.W. wrote the manuscript and prepared the figures. R.J.G., M.S.H., R.H.C., and J.D.W. supervised the project and edited the manuscript.

Competing interests: R.J.G. is an employee of Second Sight Medical Products, Inc. M.S.H. has a financial interest in and is a consultant for Second Sight Medical Products, Inc.

Data and materials availability: The pAAV2-CAG-GCaMP5G viral plasmid is available from authors J.D.W. or R.H.C.

Introduction

Age-related macular degeneration (*1*) and retinitis pigmentosa (RP) (*2*) lead to loss of retinal photoreceptor cells, causing blindness in hundreds of thousands of people each year. Retinal prosthetic implants treat these incurable conditions by electrically stimulating surviving cells in the inner retina (*3*). These devices are becoming a viable clinical option, with two systems now approved by regulatory bodies [Argus II (*4*) and Alpha IMS (*5*)]. Patients with implants can detect light and show measurable improvement in visually guided tasks such as walking along a line on the floor. This improvement benefits patients in their daily lives by, for example, increasing their confidence while walking.

Clinical studies of epiretinal and subretinal implants reveal limitations in the ability of patients to perceive shapes and forms. Most subjects cannot determine the orientation of gratings (used to measure visual acuity), and those who can recognize letters take more than 40 seconds to do so (*6, 7*). Shape perception requires precise activation of retinal cells with a two-dimensional array of electrodes that creates a spatial pattern of activity in the retina (*8*). In order to elicit a small visual phosphene that can serve as a building block for the pattern, each electrode should activate only nearby cells. In practice, however, patients receiving single-electrode stimulation often report a streak-shaped phosphene, rather than a focal spot of light (*9, 10*), and multielectrode stimulation is hindered by interactions among neighboring electrodes (*11, 12*).

Experiments with epiretinal implants have revealed that the inability to achieve focal activation arises in part from unintended stimulation of passing axons. Retinal ganglion cell (RGC) axons project from the periphery of the retina to the optic disc and pass close to the electrodes (closer than ganglion cell bodies). The stimulation of axons produces an elongated phosphene due to antidromic activation of cell bodies located peripheral to the point of stimulation (*10*). We recently compared phosphene drawings from implant patients to anatomical models of retinal axon pathways (*9*). In nearly all cases, a phosphene's length and orientation matched the trajectory of the axons that traversed the stimulating electrode. Furthermore, activating two electrodes along the same axon pathway produced only a single percept.

To investigate stimulus paradigms that provide better control over the spatial patterns of RGC activation, we developed an in vitro retinal preparation in which we could map these patterns with unprecedented spatial resolution. We designed an adeno-associated viral (AAV) vector that transduces over 80% of RGCs in the rat retina with the genetically encoded calcium indicator GCaMP5G (*13*). We then used calcium imaging to record from RGC populations in isolated retinas while stimulating with transparent multielectrode arrays (MEAs) (see Materials and Methods). Although in vitro retinal preparations have been used extensively to inform the design of retinal implants [see (*14*) for review], they have relied on single-unit (patch clamp) or MEA recordings, which capture responses from only a few cells in a confined area. Calcium imaging overcomes this limitation by permitting real-time mapping of RGC activity both in a large area and at single-cell resolution.

Results

Varying stimulus pulse duration

Prior studies have revealed that stimulus pulse parameters can dramatically influence which neural elements are activated by an electrode. For example, with regard to epiretinal cathodic stimulation, short pulses (e.g., 0.1 ms) excite RGCs preferentially, while longer pulses (e.g., 1 ms) excite both RGCs and presynaptic bipolar cells (*15*, *16*). There is, however, little information about how pulse width affects the spatial extent of RGC activation. To investigate this, we used calcium imaging to measure precisely the complete pattern of electrically activated RGCs (Fig. 1A and movie S1). With this method, we mapped RGC response patterns to a wide range of pulse widths, spanning more than three orders of magnitude (Fig. 1B and table S1). All pulses 8 ms and shorter activated axons, causing streak responses extending from the electrode to the edge of the retina [for reference, the Argus II and Alpha IMS implants have been reported to use 0.45- and 1-ms pulses, respectively (*4*, *5*)]. Sixteen-millisecond pulses also stimulated axons but to a much lesser extent (fewer than 5% of the cells ≥ 100 μm to the right of the electrode perimeter responded to stimulation). Pulses 25 ms and longer produced no evidence of axonal stimulation, instead resulting in focal activation. Threshold charge density became higher as pulse width increased, indicating that longer pulses were less efficient at evoking responses (also see fig. S2B), consistent with earlier findings (*15*, *17*).

Varying stimulus amplitude

With long stimulus pulses (≥ 25 ms), the thresholds of the cell bodies directly above the electrode were highly uniform and increased with distance from the electrode perimeter (Fig. 1C). This suggests that using long pulses could permit an amplitude coding strategy in which percept size is controlled by stimulus strength. While amplitude coding has been demonstrated in an Argus I subject with 0.45-ms pulses, higher amplitudes also stimulated passing axons (*10*). We did not observe axonal activation for pulses 25 ms or longer, regardless of amplitude (fig. S1A, inset). In spite of this encouraging result, implementing amplitude coding in the clinical setting would require improved electrode materials that allow higher electrochemically safe charge densities (see Discussion).

Of the pulse widths that produced streak responses (≤ 8 ms), a subset showed distinct threshold differences between ganglion cell bodies (Fig. 1B, cells above the electrode) and axons (Fig. 1B, cells to the right of the electrode). Consistent with prior reports (*15*, *16*), selectivity for RGC somata was relatively high (~1.7×) for the shortest pulses (0.06 and 0.1 ms) and gradually diminished (to ~1.1×) as pulse width increased to 4 ms (fig. S1A). This suggests that short pulses could achieve focal activation over a small range of stimulus amplitudes. Staying within this range would be challenging in implant patients (see Discussion).

Blocking synaptic transmission

The transition in response shape from elongated to focal occurred at a pulse width of 16 ms (Fig. 1B). We speculated that this transition represented a shift from direct to indirect activation of RGCs, such that shorter pulses stimulated RGCs directly, while longer pulses

targeted bipolar cells. To test this, we measured how thresholds at every pulse width were affected by synaptic blockers (Fig. 1D) (see Materials and Methods). We observed no change in thresholds for 0.06-ms pulses ($P = 0.09$), suggesting direct RGC activation at this pulse width. Thresholds for 0.1–8-ms pulses rose by 20–100% in the presence of blockers ($P < 0.001$), implying contributions from inner retinal stimulation. Pulses 16 ms and longer evoked no calcium transients once synaptic transmission was blocked, indicating that long pulses achieve focal activation by preferentially targeting bipolar cells, which in turn activate RGCs.

Sinusoidal stimulation

It was recently shown that 5–25-Hz sine-wave stimulation elicits responses in RGCs (either directly or indirectly) while avoiding activation of passing axons (*18*, *19*). Recordings were made from only one cell at a time via the patch clamp technique, however, so the spatial extent of the RGC responses could not be determined. We imaged RGC responses to 20-Hz sinusoidal stimulation. The response shape (Fig. 2A) was largely focal and looked similar to that of 20-Hz square waves (i.e., 25-ms pulses). Stimulation thresholds for 20-Hz sine waves were lower than those of 20-Hz square waves. We quantified these differences by imaging the same set of RGCs in two retinas during stimulation with both waveform shapes. Overall, square wave thresholds were 22.8 ± 35.5% higher than sine wave thresholds ($P < 0.001$; Fig. 2B). Though the standard deviation is relatively large, these results suggest that 20-Hz sinusoids are generally more effective at stimulating bipolar cells than square waves of the same frequency. Another study also reported lower thresholds for sine versus square waves, though at much higher stimulus frequencies (*20*).

Retinal degenerative animal model

To determine the effects of retinal degeneration (RD) on RGC response patterns, we mapped stimulation thresholds in the S334ter-line-3 rat model of RP (Fig. 3, top row). Response shapes in RD rats (aged ~P600) matched those of wild-type (WT) retina: short pulses (0.06 and 1 ms) produced streaks, while long pulses (25 ms) evoked focal responses. Soma and axon thresholds in RD retina were similar to those of WT retina for 0.06-ms pulses and slightly elevated for 1-ms pulses (table S3). With 25-ms pulses, however, RD thresholds were roughly 3 times as high as in WT retina ($P < 0.001$). These results indicate that bipolar cell thresholds increase during degeneration, while RGC thresholds remain unchanged. This finding clarifies conflicting reports of whether RD causes elevated stimulation thresholds (see Discussion).

Effect of electrode size

To achieve finer visual acuity, retinal implants must use higher-density MEAs with smaller electrodes. Thus, to inform the design of future implants, it is important to understand how response patterns are affected by electrode size. We therefore mapped stimulation thresholds with smaller-diameter electrodes (75 and 30 μm) (Fig. 3). We found that threshold charge density increased as electrodes became smaller, while response shape remained the same. The size of the response area decreased with electrode size but only to a certain extent. With 25-ms pulses, for example, 75-μm electrodes evoked responses from a smaller area than

200-μm electrodes, but no further reduction in response area was achieved with 30-μm electrodes. The apparent equivalent response between 75- and 30-μm electrodes suggests a lower limit to the spatial resolution that can be achieved with epiretinal stimulation. This limit, however, is likely smaller than the response area due to nonlinear summation in receptive field subunits (*21*).

Multielectrode pattern stimulation

Having demonstrated focal activation with a single small electrode, we next explored whether multielectrode stimulation could activate patterns of RGCs that matched the pattern of stimulation. We began by measuring electrode interactions, which are known to influence percept quality in implant patients (*11*, *12*). We observed both electric field interactions and interactions at the neural level, though neither significantly impacted the overall response shape (figs. S3 and S4). We then proceeded with a four-electrode line pattern, testing both short (0.1 ms) and long (25 ms) pulse durations. With short pulses, stimulating near threshold activated a group of ~10 cells that resembled a line (Fig. 4A, top row). However, many cells were offset from the electrodes by tens of microns in different directions [presumably due to stimulation of axon initial segments (*22*, *23*) (see Supplementary Materials)], which distorted the shape of the line. Furthermore, increasing stimulus amplitude by only 50% caused extensive axonal stimulation that completely obscured the line.

In contrast, long pulses were effective in generating RGC line patterns over a wide range of stimulus amplitudes (Fig. 4A, middle and bottom rows). Even with the electrodes situated directly along an axon bundle, stimulating well above threshold produced a line without a streak pattern. To assess whether long pulses could evoke more complex patterns, we activated groups of electrodes in the shapes of letters. We formed the letters *L*, *F*, and *T*, each of which was clearly legible (Fig. 4B). On the human retina, their height (375 μm) would correspond to 9-mm-tall letters viewed from typical reading distance and a Snellen acuity of 20/312 (*24*). This is approximately four times as high as the best visual acuity reported among Argus II users and nearly twice as high as that of Alpha IMS users (*3*).

Clinical testing in a retinal prosthesis patient

To assess the clinical validity of our findings, we examined the effect of stimulus pulse duration on phosphene shape in an epiretinal prosthesis subject (Fig. 5 and table S4) (see Materials and Methods). As expected, short pulses (0.45 ms/phase) evoked streak-shaped percepts characteristic of axonal stimulation. In comparison, long pulses (25 ms/phase) elicited small, focal percepts, indicating that axonal stimulation did not occur. These data further support our claim that long pulses produce focal percepts. Furthermore, they validate our in vitro response patterns as predictors of human shape perception.

Discussion

Clinically deployed retinal implants typically use stimulus pulses on the order of 1 ms (*4*, *5*). Our data indicate that this pulse width results in indiscriminate activation of RGC axons, causing patients to see elongated phosphenes. We demonstrate that focal responses from the

retina are best produced with stimulus pulses of 25 ms or longer. This was true in an animal model of RD as well as in a retinal implant patient, indicating that the response to electrical stimulation in the inner retinal network is minimally affected by degeneration.

There have been conflicting reports as to whether retinal degeneration causes elevated stimulation thresholds. Most animal electrophysiology studies cite higher thresholds in RD retina versus WT controls: Thresholds of rd1 mouse retinas were reported to be 1.2–7.4 times as high as those of WT retina (*20, 25*). In Royal College of Surgeons (RCS) rats, thresholds were 2–6 times higher than in WT (*26*). In P500–P700 S334ter-line-3 rats (the same age and strain used in this study), thresholds were elevated by up to 4× versus normal controls (*27*). Similarly, studies in Argus II patients found a positive correlation between electrical and light thresholds, suggesting that stimulation thresholds increase as degeneration progresses (*4*). Despite these findings, most of these studies applied pulse widths that excite both ganglion and bipolar cells. Long-latency spikes were often recorded, indicative of inner retinal stimulation. To date, only one other group has ensured direct RGC stimulation in RD retina (P23H rats) by using short pulse widths (0.05–0.1 ms) and synaptic blockers (*28*). They found that thresholds were not affected by degeneration. Collectively, these studies corroborate our finding that bipolar cell thresholds become elevated during degeneration while direct RGC thresholds remain unchanged (Fig. 3 and table S3). This may be a consequence of the extensive remodeling that affects inner retinal neurons but not RGCs (*29, 30*).

Several lines of evidence in this study suggest that long pulses target bipolar cells rather than photoreceptors (although we cannot strictly rule out activity originating in other presynaptic interneurons). First, photoreceptors were bleached by the bright fluorescence excitation light, causing them to remain hyperpolarized. This prevents the cells from releasing glutamate onto bipolar cell dendrites, effectively blocking their output. Second, the chronaxie we measured for stimulation with long pulses is similar to bipolar cell chronaxies reported by others (see Supplementary Materials). Third, and most compelling, RD retinas responded to stimulation with 25-ms pulses, even though animals were of an age associated with complete photoreceptor loss (~P600) (*31*).

It is well known that short pulses stimulate RGCs through activation of voltage-gated sodium channels (*22, 32*). Though the mechanism underlying bipolar cell responses to electrical stimulation is less clear, modeling studies have implicated L- and T-type calcium channels (*18, 33*). These channels trigger glutamate release from bipolar cells (*18*) and are thought to be activated by long-duration stimuli (i.e., low-frequency sinusoids). Bipolar cells have longer time constants than RGCs, consistent with our findings that long pulses target bipolar cells and short pulses target RGCs (*14, 34*).

Though never validated clinically, in vitro MEA recordings by Sekirnjak et al. (*35*) and Jepson et al. (*8, 23*) demonstrated that short stimulus pulses (≤ 0.1 ms) produce focal retinal activation. By using small stimulating electrodes (~10-μm diameter), the authors were able to target a single RGC (*23, 35*). We have confirmed this result with larger electrodes (30-μm diameter; fig. S3A, top row); however, increasing stimulus amplitude by only 50% above threshold activated passing axons (fig. S3A, middle row). Jepson et al. also reported axonal

stimulation but used an MEA with a diameter less than 500 μm, limiting spatial assessment (*8*, *23*). Here, we imaged more than 2 mm of retina and show that stimulating axons activates a streak of RGCs extending to the retina's edge (Fig. 1A). This effect occurs with short-pulse-width stimulation at amplitudes only ~40–130% above threshold (depending on electrode diameter; fig. S1B). Thus, there is a relatively narrow range of amplitudes for which short pulses can produce focal responses. Remaining within this range would be difficult in clinical practice (*14*). Electrical thresholds among ganglion cell types can vary by threefold (*22*), and perceptual thresholds in implant patients rise steadily during repeated stimulation (*32*).

To our knowledge, four other animal studies have investigated which retinal cell type(s) are targeted by epiretinal stimulation with pulses longer than 10 ms (*15*, *36*-*38*). Each concluded that inner retinal cells were activated by long pulses. However, direct RGC stimulation (of both cell bodies and axons) was also observed. A typical RGC response consisted of a single spike elicited by direct activation followed by a burst of spikes arising from indirect (synaptic) activation. Though we did not observe axonal responses to long pulses, it is possible that distant cells were in fact stimulated antidromically but that their spiking was too sparse to detect with GCaMP5G (see below).

Of the four studies that explored long pulses, only Jensen et al. (*15*) measured the effect of pulse width on stimulus thresholds of RGC axons. In agreement with our results, they found that short pulses (≤ 1 ms) were selective (up to 4×) for ganglion cell bodies over passing axons, while long pulses (≥ 20 ms) were selective for inner retinal cells. However, selectivity for long pulses was only 1.25–2×, considerably lower than what we observed (see fig. S1A, inset). This led Jensen et al. to conclude that short pulses are best for avoiding axons, a finding that contradicts our own. This contradiction most likely arises from the different recording techniques used in each study. Jensen et al. relied on electrical recordings, which could detect any single, short-latency spikes elicited in axons. However, a single spike would go undetected by GCaMP5G, causing our long-pulse selectivity measurements to be much higher than those of Jensen et al.

Generation of both short and long pulses is challenging from an engineering perspective, but for different reasons. Short pulses (≤ 0.1 ms) require large amounts of electrical charge to be delivered quickly. This requires high voltages and thus larger implant components. Long pulses require even more charge (fig. S2B), placing demands on the electrode material used for stimulation. Although thresholds for 25-ms pulses were below the electrochemical safety limit of platinum [0.35 mC/cm^2 (*39*)] for 75- and 200-μm-diameter electrodes, this may not be the case with human implants, where separation between the MEA and retina (up to several hundred microns) can cause a dramatic increase in thresholds (*4*).

Another apparent disadvantage of long pulses is that they do not permit the high-frequency stimulation required for rate coding. However, clinical testing has revealed that subretinal implant patients tend to prefer low stimulus frequencies (5–7 Hz) (*5*, *7*, *19*). Furthermore, the need for rate coding may be obviated since stimulation of bipolar cells causes postsynaptic RGCs to fire bursts of spikes (*34*, *40*). These bursts may represent the natural

firing patterns of ganglion cells in response to a spot of light (*34*). The number and timing of spikes in a burst can be controlled through stimulus amplitude and pulse duration (*34*).

Others have argued that bipolar cell stimulation may be ineffective because responses quickly become desensitized (*21, 40, 41*). These studies used maximum pulse durations of 1–4 ms, however. It is not known whether desensitization occurs with much longer pulses (e.g., 25 ms). The only studies to measure spike rates during repetitive stimulation with long-duration waveforms (5–25-Hz sinusoids) did not report any effects of desensitization (*18, 19*). A modeling study by the same group predicted that calcium channels, which underlie synaptic release from bipolar cells, respond robustly to repetitive sine-wave stimulation in this frequency range (*33*).

Although we could not test long pulses in Argus II patients (because of current system limitations), we can use the Argus I results to estimate Argus II thresholds for 25-ms pulses. Twenty-five-ms pulses with a stimulus amplitude of 0.73 mC/cm^2 elicited phosphenes on a subset of the Argus I patient's 260-μm-diameter electrodes (see Materials and Methods), thus providing an estimate of threshold charge density. Assuming that threshold charge remains constant (*42*), a 200-μm-diameter Argus II electrode should have a threshold charge density of 1.23 mC/cm^2 (a result of its ~40% smaller surface area versus a 260-μm-diameter electrode). This is above the published Argus II safety limits for acute and chronic stimulation (1.0 and 0.35 mC/cm^2, respectively); however, these limits were determined for stimulation with short pulses (0.45 ms) (*4*). Long pulses allow higher electrochemically safe charge densities, since reversible reactions have more time to proceed. Electrochemical measurements (see Materials and Methods) indicate that 25-ms pulses have a charge injection limit 3.5 times as high as that of 0.45-ms pulses (fig. S5), corresponding to a charge density limit of 1.23 mC/cm^2 for chronic stimulation. Thus, the predicted stimulus threshold for Argus II electrodes with long pulses is equal to the predicted electrochemical safety limit. If this estimate is borne out in clinical testing, then the utility of long pulses will be limited. Furthermore, many electrodes in Argus II patients are several hundred microns from the retina, which further increases thresholds (*4*). One way to mitigate this problem is to gang electrodes by applying pulses simultaneously on adjacent channels, effectively increasing the surface area of stimulation. This strategy has proven effective in a clinical setting to overcome the problem of thresholds near safety limits (*43*); however, it also stimulates a larger area of retina, thereby decreasing resolution. In summary, the applicability of long-pulse stimulation in Argus II patients may be limited, although direct experimentation should be done to confirm this prediction.

Utilizing long pulses in future retinal prostheses will require adoption of advanced electrode materials (*44*) to safely apply increased charge density. This is particularly important if devices use smaller electrodes (Fig. 3) and amplitude coding (Fig. 1C), since both require higher charge densities. One promising electrode material is iridium oxide (IrO_2). Sputtered IrO_2 films have electrochemical limits up to 9 mC/cm^2 for 1-ms pulses (and potentially higher limits for longer pulses) (*44*). In addition to improved electrode materials, more flexible substrates are needed to consistently position electrodes close to the retina and thereby achieve low and predictable thresholds. Ahuja et al. found that 80.9% of Argus II electrodes in contact with the macula had thresholds below 0.35 mC/cm^2 (*4*). To further

reduce thresholds, sinusoidal stimulation can be used as an alternative to pulsatile stimulation (Fig. 2).

Our results are limited by the fact that detectable changes in calcium indicator fluorescence required a burst of at least five spikes from the RGC (*13*). A single action potential elicited by a stimulus would therefore go undetected. To address this, we applied a train of stimulus pulses to elicit a train of spikes. Train stimuli are also used in clinical trial threshold measurements, thus making for a good comparison between the in vitro and human data. However, the lack of sensitivity may confound our finding that long pulses do not stimulate axons of passage. It is possible that long pulses elicited a single spike in axons without accumulating enough calcium to generate a rise in fluorescence. Future studies with the more sensitive GCaMP6 indicator (*45*) may be able to resolve this question. In any case, our threshold maps clearly indicate that the largest concentration of spiking activity occurs near the stimulating electrode. Coupled with our human patient data showing that longer-duration stimuli cause rounder percepts (Fig. 5 and table S4), it likely that the large number of bursting RGCs near the electrode dominates the perceptual response.

We have shown that multielectrode stimulation with long pulses produces activation areas consistent with the stimulus pattern, suggesting that form vision can be achieved at much higher resolution than currently available. Our in vitro data indicate that a visual acuity of ~20/300 may be possible, consistent with a recent study demonstrating 20/250 through subretinal stimulation in a rodent model (*21*). This is in contrast to a best reported acuity of 20/1260 with the Argus II and 20/546 with the subretinal Alpha IMS (*3*). The threshold for legal blindness is 20/200, so even if the results of our study translate to clinical measurements when higher-resolution devices become available, patients would still be considered blind. Nevertheless, 20/300 is a considerable improvement over simple light perception vision.

Our findings support engineering development needed to incorporate long-pulse-width stimulation into clinical devices, including subretinal implants. The only clinically approved subretinal prosthesis, the Alpha IMS, uses a pulse duration of 1 ms (*5*). Though this device is designed to stimulate bipolar cells, which lie in close proximity to the electrodes, in vitro animal studies have found that subretinal stimulation with 1-ms pulses also activates RGCs directly at thresholds statistically similar to those of inner retinal cells (*37, 38, 46*). These studies were performed in healthy retina with pulse durations up to 10 ms. As we have shown, bipolar cell (but not RGC) thresholds become elevated during retinal degeneration (Fig. 3 and table S3). This suggests that in RD retina, RGC thresholds to subretinal stimulation may be *lower* than bipolar cell thresholds. For these reasons, others have proposed that subretinal stimulation (at least with pulse durations up to 10 ms) can activate RGC axons (*14*) [however, see also (*47, 48*)]. Thus, our finding that pulses 25 ms and longer avoid axonal stimulation may have important implications for the design of both subretinal and epiretinal implants.

In summary, we demonstrate a technique for producing focal perceptions with retinal prostheses. The mechanism is explored with an in vitro retinal preparation that enables simultaneous recording from hundreds of RGCs. Experiments showed a response area

limited to RGCs near the stimulating electrode. Focal perceptions were confirmed in an epiretinal prosthesis patient. Our findings predict that form vision is indeed possible, thus providing strong evidence to support development of high-resolution retinal prostheses.

Materials and Methods

Study design

This study was designed to investigate electrical stimulation strategies that enable better control over the shapes of percepts elicited by retinal implants. Our goal was to find a single-electrode stimulus that produced a focal percept, thereby enabling pattern activation of the retina during multielectrode stimulation. To search for such a stimulus, we performed calcium imaging of RGC populations in isolated rat retina during electrical stimulation with MEAs. Animals were given an intravitreal injection of an AAV vector that encoded the genetically encoded calcium indicator GCaMP5G. After gene expression occurred, retinas were dissected out, mounted on a transparent MEA and stimulated with one or more electrodes while imaging evoked calcium transients with an inverted fluorescence microscope.

We systematically investigated the effect of stimulus pulse width, electrode size, and retinal degeneration on RGC response patterns. For each set of stimulus parameters, ganglion cell thresholds were mapped in space with respect to the stimulating electrode position. Each threshold map was required to contain recordings from at least 1,000 RGCs in 3 or more retinas (see table S2 for details). After the single-electrode stimulation experiments, multielectrode stimulation was performed to assess the potential for high-resolution pattern activation of the retina. We concluded the study by testing the effect of stimulus pulse width on percept shape in an epiretinal prosthesis patient.

Animal models

Wild-type Long Evans rats (aged P81–P260, $n = 15$) were purchased from Harlan Laboratories. S334ter-line-3 rats (aged P591, P611, and P619) with retinal degeneration were bred in-house by crossing homozygous breeders (a gift from M. LaVail, University of California, San Francisco) with Copenhagen rats (Charles River Laboratories International). S334ter is a mutation that causes truncation of the rhodopsin protein, and the animals carrying this mutation are good models of autosomal dominant RP. Heterozygous animals undergo a slower degeneration than homozygous strains and are therefore a better model of human RP (*28*). The animals were used at an age at which their photoreceptors were completely degenerated and their retinas had undergone considerable reorganization, resembling late-stage human RP (*31*). Absence of light flash responses was confirmed in isolated RD retinas at the beginning of each experiment. All procedures were approved by the Institutional Animal Care and Use Committee and the Institutional Biosafety Committee at the University of Southern California (USC).

AAV production

Recombinant AAV2-CAG-GCaMP5G was produced at the University of Florida Vector Core by the two-plasmid cotransfection method (*13*). Final titer was 3.2×10^{12} vector

genomes per milliliter (vg/mL). A prior study with AAV2-CAG-GCaMP5G indicated that the virus transduces roughly 85% of rat RGCs with high specificity after intravitreal injection (*13*). A minority of infected cells (~15%) are displaced amacrine cells, which constitute roughly half the cells in the ganglion cell layer. To limit GCaMP overexpression and cytomorbidity (*13*), viral stock was diluted in balanced salt solution to 4.9×10^{11} vg/mL prior to injection.

Intravitreal AAV administration

Animals were anesthetized with intraperitoneal injection of ketamine (60 mg/kg) and xylazine (8 mg/kg). Phenylephrine (2.5%) and tropicamide (1%) were dropped into each eye to induce pupil dilation. Tetracaine (0.5%) was applied as a local anesthetic. A 30-gauge needle was used to make a pilot hole through the sclera, choroid, and retina, 1–2 mm posterior to the corneal limbus. A microliter syringe (Hamilton) attached to a blunt 32-gauge needle was used to inject 4 μL of AAV2-CAG-GCaMP5G into the vitreous of each eye over a 30-s period. After injection, the needle was left in place for 30 s and withdrawn slowly to prevent leakage. Antibiotic eye ointment was applied to prevent infection.

Retina preparation and dye loading

Retinas were harvested 2–4 weeks after injecting AAV2-CAG-GCaMP5G into the vitreous cavities. Since the extent of GCaMP5G transduction depended on the quality of injection (*13*), retinas from both eyes were kept alive until their expression profiles could be examined. All RGCs were labeled with a red fluorescent dye to determine which GCaMP5G-expressing cells were RGCs (as opposed to displaced amacrine cells).

Rats were deeply anesthetized with ketamine (60 mg/kg) and xylazine (8 mg/kg). The first eye was enucleated, and the optic nerve was trimmed to 0.5 mm in length. A segment of thin-wall polyimide tubing was glued around the nerve to create a chamber. The eye was then submerged in calcium-free Ames' Medium (*13*) (to prevent calcium-dependent resealing of the optic nerve) and hemisected. Vitreous was removed with a custom extractor (*17*) to allow tight coupling between the retina and MEA. The posterior eyecup was transferred to a Petri dish, and the red tracer dye Alexa 594 hydrazide sodium salt (30 mM, 1.5 μL; Life Technologies) was pipetted into the polyimide tubing to cover the cut RGC axons. The eyecup was then placed in a perfusion chamber for 1 h to allow retrograde diffusion of the dye into RGC somata. During dye loading, the eyecup was superfused with bicarbonate-buffered Ames' Medium at 30 °C and a flow rate of 4–5 mL/min. Media was supplemented with penicillin-streptomycin, adjusted to 280 mOsm, and equilibrated with 5% CO_2/95% O_2 gas. Shortly after transferring the first eye to the perfusion chamber, the rat was rapidly decapitated, and all procedures were repeated on the second eye.

Imaging and electrophysiology

After dye loading, each retina was dissected out and mounted on a porous Teflon membrane (#JVWP01300; Millipore) attached to a titanium ring. The assembly was inverted and placed on an MEA such that the inner retinal surface contacted the substrate. The MEA was then transferred to an inverted microscope (Eclipse TE2000-U; Nikon) to examine GCaMP5G expression profiles. Only retinas containing dense and widespread expression

were used for recording. In most cases, a smaller section of retina (~5×5 mm) was used, as larger pieces did not lie flat on the MEA. The optic disc was always kept intact so that its position could be identified during data processing. Throughout each experiment, the retina was superfused with Ames' Medium at a flow rate of 4–5 mL/min and a temperature of 33 °C.

Fluorescence excitation was provided by a super bright white LED. Excitation and emission light were filtered through Semrock filter sets: #GFP-4050A for GCaMP5G and #TXRED-4040B for Alexa Fluor 594. Images were viewed through a Nikon Plan Apo 0.75-NA 20× objective and captured by an Andor Technology iXon electron-multiplied CCD camera at 5 Hz (85% exposure duty cycle).

Multielectrode arrays were fabricated at the W. M. Keck Photonics Laboratory at USC, a class 100 cleanroom. Each MEA contained 60 disc electrodes ranging from 30 to 200 μm in diameter. Arrays were constructed from thin, transparent materials (glass, indium tin oxide, silicon nitride, and SU-8 epoxy photoresist) to permit imaging through the substrate. Some electrodes were plated with platinum/iridium by cyclic voltammetry to increase charge injection limits.

Electrical stimuli consisted of charge-balanced, biphasic current waveforms. Voltage stimuli were delivered by a computer-controlled stimulus generator (STG2008; Multi Channel Systems) and fed through a custom voltage-to-current converter. Signals were relayed to MEA electrodes through a custom interface board. A platinum wire encircling the top of the recording chamber served as the return electrode.

All stimuli were repetitive to evoke a burst of spikes and generate a detectable calcium transient (*13*). Rectangular pulse trains, square waves, and sine waves were applied in different settings (depending on pulse width). Stimuli were always cathodic-first, with individual pulse durations ranging from 0.06 to 100 ms. All stated amplitude and pulse width values are for the cathodic phase only.

Table S1 provides the stimulus waveform parameters for every pulse width. The length of each stimulus was limited to a single image frame (≤ 200 ms) in order to appear instantaneous relative to the rate of image acquisition. Pulses ≤ 2 ms were delivered as 167-Hz rectangular pulse trains. To remain consistent with prior studies (*16, 17, 28*), each pulse began with a cathodic phase followed by an anodic phase of twice the duration and half the amplitude. Pulses longer than 2 ms required symmetric square waves, as the 200-ms time window was not long enough to permit asymmetric pulses or interpulse gaps.

A control experiment was performed to verify that response shape depended only on leading pulse width and not on other stimulus parameters. Response patterns were found to be spatially consistent for a given pulse width, regardless pulse symmetry or interpulse delay. For example, 500-Hz trains of symmetric 1-ms pulses activated the same RGCs as 167-Hz trains of asymmetric 1-ms pulses. Similarly, 10-Hz trains of asymmetric 25-ms pulses activated the same RGCs as 20-Hz square waves (i.e., trains of symmetric 25-ms pulses).

Threshold measurements

Ten-minute stimulus protocols were used to measure thresholds of every transduced RGC in a given field of view. Current of progressively increasing amplitude was delivered to the retina while imaging GCaMP5G fluorescence. A total of 10 amplitudes were used, each lasting 1 min. For each amplitude, 14 identical stimuli were delivered on 3.6-s intervals (stimuli were repeated to obtain redundancy and reduce detection noise). Electrically evoked responses were detected by high-pass filtering of the fluorescence intensity of each ganglion cell body and identifying rapid changes in fluorescence temporally correlated with the stimuli. To calculate thresholds, a dose-response curve was generated for every RGC by plotting the fraction of the 14 stimuli that elicited a response at each amplitude. A sigmoidal function was fit to each curve, and threshold was defined as the amplitude that yielded a 50% response. Charge density was used as a measure of threshold, since its value accounts for electrode size, pulse width, and waveform shape.

Spatial threshold maps (Figs. 1B, 2A, and 3) were generated by binning cells in a grid according to their location relative to the stimulating electrode. Thresholds of cells in each grid bin (30×30 μm) were averaged. Maps from separate retinas or from different fields of view in the same retina were combined by rotating and shifting each into the same reference frame (relative to the optic disc and electrode position) and averaging. Table S2 lists the number of responding and non-responding RGCs that make up each threshold map. (Maps were generated only from cells double-labeled with GCaMP5G and Alexa 594 to ensure that they were RGCs.) All data processing was performed in ImageJ (National Institutes of Health) and MATLAB (MathWorks). Except for marking ganglion cell body locations, processing steps were automated and identical for each data set.

Background-subtracted images

The large fluorescence signals provided by GCaMP5G enabled visualization of raw patterns of stimulus-evoked RGC activity. Background-subtracted fluorescence images (see Fig. 1A for an example) were generated by subtracting baseline fluorescence (acquired before stimulation) from images recorded during and/or immediately after stimulation. Brightness and contrast were globally adjusted to accentuate the responses.

Blocking synaptic transmission

CNQX (70 μM, AMPA/kainite receptor antagonist), D-APV (50 μM, NMDA receptor antagonist), and L-APB (50 μM, mGluR6 receptor agonist) were used to block excitatory input to RGCs, while strychnine (10 μM, glycine receptor antagonist) and picrotoxin (50 μM, $GABA_A$ receptor antagonist) were applied to block inhibitory input (*30*). All blockers were dissolved in the superfusate and were washed in for at least 10 minutes prior to recording. CNQX has poor water solubility and was therefore dissolved in DMSO before being added to the superfusate (final DMSO concentration was 0.1%). Lack of synaptic transmission was verified by confirming absence of light responses.

Human psychophysical experiments

Data were collected from a single subject, blind with RP, chronically implanted with a 16-channel epiretinal prosthesis [Argus I (*4*)] as part of a clinical trial (clinicaltrials.gov identifier NCT00279500). (Data could not be acquired from Argus II subjects, as system limitations did not permit stimulation with pulses longer than 10 ms.) All tests were performed after obtaining informed consent under a protocol approved by the USC Institutional Review Board and in compliance with the Declaration of Helsinki.

The Argus I electrode array was implanted in the macular region of the subject's retina. The MEA contains two electrode sizes: 260- and 520-μm diameter, subtending 0.9° and 1.8° of visual angle, respectively. Data were acquired by asking the subject to draw the phosphene elicited when each electrode was activated separately. Percept drawings for a given electrode were collected in random order, up to 5 times per pulse duration, amongst other single-electrode test stimuli.

Stimulation consisted of short (0.45 ms/phase) or long (25 ms/phase) cathodic-first biphasic pulses, each delivered at 20 Hz for a 500-ms duration. For short pulses, stimulus amplitude was held between 1.7 and 2 times the phosphene perceptual threshold. Since long pulses have relatively high threshold charge densities (see fig. S2B), these pulses were presented as sinusoidal waveforms, which have lower thresholds than square waves (see Fig. 2). Pseudo-sinusoids (Fig. 5A) were used because the Argus I hardware does not permit stimulation with true sine waves. Pseudo-sinusoid stimulus amplitude was fixed at 24 μA (the maximum permitted by the system for this type of stimulation), corresponding to charge densities of 0.18 and 0.73 mC/cm^2 for 520- and 260-μm-diameter electrodes, respectively. At this amplitude, 5 of the 16 MEA electrodes elicited phosphenes during at least 1 of the 5 stimulus presentations (see table S4).

After each stimulus presentation, the subject drew the percept on a grid screen with a tracking tipped pen. The drawings were captured by a head-mounted camera and were used to create binary images of the phosphenes. These images were then aligned across their centers of mass, since the absolute location of the percept varies as a function of eye position. The degree of phosphene elongation was quantified by fitting an ellipse to each binary image and calculating the minor-to-major axis ratio (table S4).

Electrochemical measurements

Electrochemical testing was conducted to measure the charge injection limits for short and long pulses. Stimulation was performed with a custom platinum/iridium (80/20%) needle electrode with an exposed tip diameter of 250 μm (FHC), immersed in room-temperature phosphate buffered saline. A large-surface-area platinum wire served as the return electrode. Charge-balanced, biphasic, cathodic-first current stimuli were delivered by a stimulus generator (STG2008; Multi Channel Systems) while recording the potential excursions with an oscilloscope (Tektronix). Short pulses (0.46 ms/phase; 1 ms interphase gap) were presented at 100 Hz and long pulses (25 ms/phase; 10 ms interphase gap) at 2 Hz. For each pulse width, the maximum cathodic potential was measured for a range of stimulus amplitudes (corresponding to charge densities between 0.1 and 0.8 mC/cm^2) (see fig. S5).

[Maximum cathodic potential was taken as the voltage at the beginning of the interphase gap (when I = 0), since this value is independent of the access voltage (*49*).] The charge injection limit was defined as the charge density at which the maximum cathodic potential crossed •0.6 V, the voltage at which H_2 irreversibly evolves (*49*). All measurements were performed after several seconds of pulsing in order to obtain a steady-state response (*44*).

Statistical analysis

Each threshold map contains recordings from at least 1,250 RGCs in 3 or 4 animal retinas (see table S2 for details). Mean thresholds were calculated by averaging RGC thresholds within and across each retina. When comparing differences in mean thresholds, a linear mixed model that accounted for animal clusters was used to determine adjusted means and *P* values (all reported means are unadjusted). Generalized estimating equations with a linear scale were used to analyze data that were not normally distributed while accounting for multiple observations within each rat. Statistical significance of data in Fig. 1D and table S4 was determined with paired and unpaired t-tests, respectively. All statistical analysis was performed in SAS version 9.4 (SAS Institute) using two-sided tests and $\alpha = 0.05$. When fitting curves, fits were weighted with the reciprocal of the variance and were optimized to minimize sum of squared error.

Supplementary Material

Refer to Web version on PubMed Central for supplementary material.

Acknowledgments

Homozygous S334ter-line-3 rats were donated by M. LaVail (University of California, San Francisco). GCaMP5G cDNA was a gift from L. Looger and J. Akerboom of the Howard Hughes Medical Institute. We thank W. Hauswirth and V. Chiodo, University of Florida, for producing AAV2 vector and A. Petrossians, University of Southern California, for help with electroplating. We also thank C. Park and C. Lane, University of Southern California, for their assistance with statistical analysis.

Funding: NSF grant EEC-0310723 (M.S.H.), NIH grant 1R01EY022931 (J.D.W./R.H.C.), NIH grant R01 GM85791 (R.H.C.), Beckman Initiative for Macular Research grant 157370747 (R.H.C.), NIH grant UL1TR000130, and Second Sight Medical Products, Inc.

References and Notes

1. Jager RD, Mieler WF, Miller JW. Age-related macular degeneration. N. Engl. J. Med. 2008; 358:2606–2617. [PubMed: 18550876]
2. Hartong DT, Berson EL, Dryja TP. Retinitis pigmentosa. Lancet. 2006; 368:1795–1809. [PubMed: 17113430]
3. Zrenner E. Fighting blindness with microelectronics. Sci. Transl. Med. 2013; 5:210ps16.
4. Ahuja AK, Behrend MR. The Argus II^{TM} retinal prosthesis: Factors affecting patient selection for implantation. Prog. Retin. Eye Res. 2013; 36:1–23. [PubMed: 23500412]
5. Stingl K, Bartz-Schmidt KU, Besch D, Braun A, Bruckmann A, Gekeler F, Greppmaier U, Hipp S, Hörtdörfer G, Kernstock C, Koitschev A, Kusnyerik A, Sachs H, Schatz A, Stingl KT, Peters T, Wilhelm B, Zrenner E. Artificial vision with wirelessly powered subretinal electronic implant alpha-IMS. Proc. R. Soc. B. 2013; 280:20130077.
6. da Cruz L, Coley BF, Dorn J, Merlini F, Filley E, Christopher P, Chen FK, Wuyyuru V, Sahel J, Stanga P, Humayun M, Greenberg RJ, Dagnelie G. The Argus II epiretinal prosthesis system allows

letter and word reading and long-term function in patients with profound vision loss. Br. J. Ophthalmol. 2013; 97:632–636. [PubMed: 23426738]

7. Zrenner E, Bartz-Schmidt KU, Benav H, Besch D, Bruckmann A, Gabel VP, Gekeler F, Greppmaier U, Harscher A, Kibbel S, Koch J, Kusnyerik A, Peters T, Stingl K, Sachs H, Stett A, Szurman P, Wilhelm B, Wilke R. Subretinal electronic chips allow blind patients to read letters and combine them to words. Proc. R. Soc. B. 2011; 278:1489–1497.
8. Jepson LH, Hottowy P, Weiner GA, Daþrowski W, Litke AM, Chichilnisky EJ. High-fidelity reproduction of spatiotemporal visual signals for retinal prosthesis. Neuron. 2014; 83:1–6. [PubMed: 24991948]
9. Nanduri, D. thesis. University of Southern California; Los Angeles, CA: 2011.
10. Nanduri D, Fine I, Horsager A, Boynton GM, Humayun MS, Greenberg RJ, Weiland JD. Frequency and amplitude modulation have different effects on the percepts elicited by retinal stimulation. Invest. Ophthalmol. Vis. Sci. 2012; 53:205–214. [PubMed: 22110084]
11. Horsager A, Greenberg RJ, Fine I. Spatiotemporal interactions in retinal prosthesis subjects. Invest. Ophthalmol. Vis. Sci. 2010; 51:1223–1233. [PubMed: 19741248]
12. Horsager A, Boynton GM, Greenberg RJ, Fine I. Temporal interactions during paired-electrode stimulation in two retinal prosthesis subjects. Invest. Ophthalmol. Vis. Sci. 2011; 52:549–557. [PubMed: 20720224]
13. Weitz AC, Behrend MR, Lee NS, Klein RL, Chiodo VA, Hauswirth WW, Humayun MS, Weiland JD, Chow RH. Imaging the response of the retina to electrical stimulation with genetically encoded calcium indicators. J. Neurophysiol. 2013; 109:1979–1988. [PubMed: 23343890]
14. Freeman DK, Rizzo JF, Fried SI. Encoding visual information in retinal ganglion cells with prosthetic stimulation. J. Neural Eng. 2011; 8:035005. [PubMed: 21593546]
15. Jensen RJ, Ziv OR, Rizzo JF. Thresholds for activation of rabbit retinal ganglion cells with relatively large, extracellular microelectrodes. Invest. Ophthalmol. Vis. Sci. 2005; 46:1486–1496. [PubMed: 15790920]
16. Behrend MR, Ahuja AK, Humayun MS, Chow RH, Weiland JD. Resolution of the epiretinal prosthesis is not limited by electrode size. IEEE Trans. Neural Syst. Rehabil. Eng. 2011; 19:436–441. [PubMed: 21511569]
17. Sekirnjak C, Hottowy P, Sher A, Dabrowski W, Litke A, Chichilnisky E. Electrical stimulation of mammalian retinal ganglion cells with multielectrode arrays. J. Neurophysiol. 2006; 95:3311–3327. [PubMed: 16436479]
18. Freeman DK, Eddington DK, Rizzo JF, Fried SI. Selective activation of neuronal targets with sinusoidal electric stimulation. J. Neurophysiol. 2010; 104:2778–2791. [PubMed: 20810683]
19. Twyford P, Fried S. The retinal response to sinusoidal electrical stimulation. IEEE Trans. Neural Syst. Rehabil. Eng. 2015; PP:1–11.
20. Suzuki S, Humayun MS, Weiland JD, Chen SJ, Margalit E, Piyathaisere DV, de Juan E Jr. Comparison of electrical stimulation thresholds in normal and retinal degenerated mouse retina. Jpn. J. Ophthalmol. 2004; 48:345–349. [PubMed: 15295659]
21. Lorach H, Goetz G, Smith R, Lei X, Mandel Y, Kamins T, Mathieson K, Huie P, Harris J, Sher A, Palanker D. Photovoltaic restoration of sight with high visual acuity. Nat. Med. 2015; 21:476–482. [PubMed: 25915832]
22. Fried SI, Lasker ACW, Desai NJ, Eddington DK, Rizzo JF. Axonal sodium-channel bands shape the response to electric stimulation in retinal ganglion cells. J. Neurophysiol. 2009; 101:1972–1987. [PubMed: 19193771]
23. Jepson LH, Hottowy P, Mathieson K, Gunning DE, Daþrowski W, Litke AM, Chichilnisky EJ. Focal electrical stimulation of major ganglion cell types in the primate retina for the design of visual prostheses. J. Neurosci. 2013; 33:7194–7205. [PubMed: 23616529]
24. Drasdo N, Fowler CW. Non-linear projection of the retinal image in a wide-angle schematic eye. Br. J. Ophthalmol. 1974; 58:709–714. [PubMed: 4433482]
25. Jensen RJ, Rizzo JF. Activation of ganglion cells in wild-type and rd1 mouse retinas with monophasic and biphasic current pulses. J. Neural Eng. 2009; 6:035004. [PubMed: 19458401]

26. Mathieson K, Loudin J, Goetz G, Huie P, Wang L, Kamins TI, Galambos L, Smith R, Harris JS, Sher A, Palanker D. Photovoltaic retinal prosthesis with high pixel density. Nature Photon. 2012; 6:391–397.
27. Chan LLH, Lee EJ, Humayun MS, Weiland JD. Both electrical stimulation thresholds and SMI-32-immunoreactive retinal ganglion cell density correlate with age in S334ter line 3 rat retina. J. Neurophysiol. 2011; 105:2687–2697. [PubMed: 21411561]
28. Sekirnjak C, Hulse C, Jepson LH, Hottowy P, Sher A, Dabrowski W, Litke AM, Chichilnisky E. Loss of responses to visual but not electrical stimulation in ganglion cells of rats with severe photoreceptor degeneration. J. Neurophysiol. 2009; 102:3260. [PubMed: 19726725]
29. Mazzoni F, Novelli E, Strettoi E. Retinal ganglion cells survive and maintain normal dendritic morphology in a mouse model of inherited photoreceptor degeneration. J. Neurosci. 2008; 28:14282–14292. [PubMed: 19109509]
30. Margolis DJ, Newkirk G, Euler T, Detwiler PB. Functional stability of retinal ganglion cells after degeneration-induced changes in synaptic input. J. Neurosci. 2008; 28:6526–6536. [PubMed: 18562624]
31. Ray A, Sun GJ, Chan L, Grzywacz NM, Weiland J, Lee E-J. Morphological alterations in retinal neurons in the S334ter-line3 transgenic rat. Cell Tissue Res. 2010; 339:481–491. [PubMed: 20127257]
32. Weitz AC, Behrend MR, Ahuja AK, Christopher P, Wei J, Wuyyuru V, Patel U, Greenberg RJ, Humayun MS, Chow RH, Weiland JD. Interphase gap as a means to reduce electrical stimulation thresholds for epiretinal prostheses. J. Neural Eng. 2014; 11:016007. [PubMed: 24654269]
33. Freeman DK, Jeng JS, Kelly SK, Hartveit E, Fried SI. Calcium channel dynamics limit synaptic release in response to prosthetic stimulation with sinusoidal waveforms. J. Neural Eng. 2011; 8:046005. [PubMed: 21628768]
34. Lee SW, Eddington DK, Fried SI. Responses to pulsatile subretinal electric stimulation: effects of amplitude and duration. J. Neurophysiol. 2013; 109:1954–1968. [PubMed: 23343891]
35. Sekirnjak C, Hottowy P, Sher A, Dabrowski W, Litke AM, Chichilnisky EJ. High-resolution electrical stimulation of primate retina for epiretinal implant design. J. Neurosci. 2008; 28:4446–4456. [PubMed: 18434523]
36. Margalit E, Thoreson WB. Inner retinal mechanisms engaged by retinal electrical stimulation. Invest. Ophthalmol. Vis. Sci. 2006; 47:2606–2612. [PubMed: 16723477]
37. Boinagrov D, Pangratz-Fuehrer S, Goetz G, Palanker D. Selectivity of direct and network-mediated stimulation of the retinal ganglion cells with epi-, sub- and intraretinal electrodes. J. Neural Eng. 2014; 11:026008. [PubMed: 24608166]
38. Eickenscheidt M, Jenkner M, Thewes R, Fromherz P, Zeck G. Electrical stimulation of retinal neurons in epiretinal and subretinal configuration using a multicapacitor array. J. Neurophysiol. 2012; 107:2742–2755. [PubMed: 22357789]
39. Brummer SB, Turner MJ. Electrical stimulation with Pt electrodes: II—estimation of maximum surface redox (theoretical non-gassing) limits. IEEE Trans. Biomed. Eng. 1977; 24:440–443. [PubMed: 892838]
40. Freeman DK, Fried SI. Multiple components of ganglion cell desensitization in response to prosthetic stimulation. J. Neural Eng. 2011; 8:016008. [PubMed: 21248379]
41. Jensen RJ, Ziv OR, Rizzo JF, Scribner D, Johnson L. Spatiotemporal aspects of pulsed electrical stimuli on the responses of rabbit retinal ganglion cells. Exp. Eye Res. 2009; 89:972–979. [PubMed: 19766116]
42. de Balthasar C, Patel S, Roy A, Freda R, Greenwald S, Horsager A, Mahadevappa M, Yanai D, McMahon MJ, Humayun MS. Factors affecting perceptual thresholds in epiretinal prostheses. Invest. Ophthalmol. Vis. Sci. 2008; 49:2303–2314. [PubMed: 18515576]
43. Ayton LN, Blamey PJ, Guymer RH, Luu CD, Nayagam DAX, Sinclair NC, Shivdasani MN, Yeoh J, McCombe MF, Briggs RJ, Opie NL, Villalobos J, Dimitrov PN, Varsamidis M, Petoe MA, McCarthy CD, Walker JG, Barnes N, Burkitt AN, Williams CE, Shepherd RK, Allen PJ. First-in-human trial of a novel suprachoroidal retinal prosthesis. PLoS ONE. 2014; 9:e115239. [PubMed: 25521292]

44. Cogan SF, Ehrlich J, Plante TD, Smirnov A, Shire DB, Gingerich M, Rizzo JF. Sputtered iridium oxide films for neural stimulation electrodes. J. Biomed. Mater. Res. Part B Appl. Biomater. 2009; 89:353–361. [PubMed: 18837458]

45. Chen TW, Wardill TJ, Sun Y, Pulver SR, Renninger SL, Baohan A, Schreiter ER, Kerr RA, Orger MB, Jayaraman V, Looger LL, Svoboda K, Kim DS. Ultrasensitive fluorescent proteins for imaging neuronal activity. Nature. 2013; 499:295–300. [PubMed: 23868258]

46. Tsai D, Morley JW, Suaning GJ, Lovell NH. Direct activation and temporal response properties of rabbit retinal ganglion cells following subretinal stimulation. J. Neurophysiol. 2009; 102:2982–2993. [PubMed: 19741103]

47. Mandel Y, Goetz G, Lavinsky D, Huie P, Mathieson K, Wang L, Kamins T, Galambos L, Manivanh R, Harris J, Palanker D. Cortical responses elicited by photovoltaic subretinal prostheses exhibit similarities to visually evoked potentials. Nat. Commun. 2013; 4:1–9.

48. Fransen JW, Pangeni G, Pardue MT, McCall MA. Local signaling from a retinal prosthetic in a rodent retinitis pigmentosa model in vivo. J. Neural Eng. 2014; 11:046012. [PubMed: 24940618]

49. Cogan SF, Troyk PR, Ehrlich J, Gasbarro CM, Plante TD. The influence of electrolyte composition on the *in vitro* charge-injection limits of activated iridium oxide (AIROF) stimulation electrodes. J. Neural Eng. 2007; 4:79. [PubMed: 17409482]

50. Schiefer MA, Grill WM. Sites of neuronal excitation by epiretinal electrical stimulation. IEEE Trans. Neural Syst. Rehabil. Eng. 2006; 14:5–13. [PubMed: 16562626]

One Sentence Summary

The spatial resolution of retinal implants in blind individuals can be vastly improved by using long-pulse-duration stimuli.

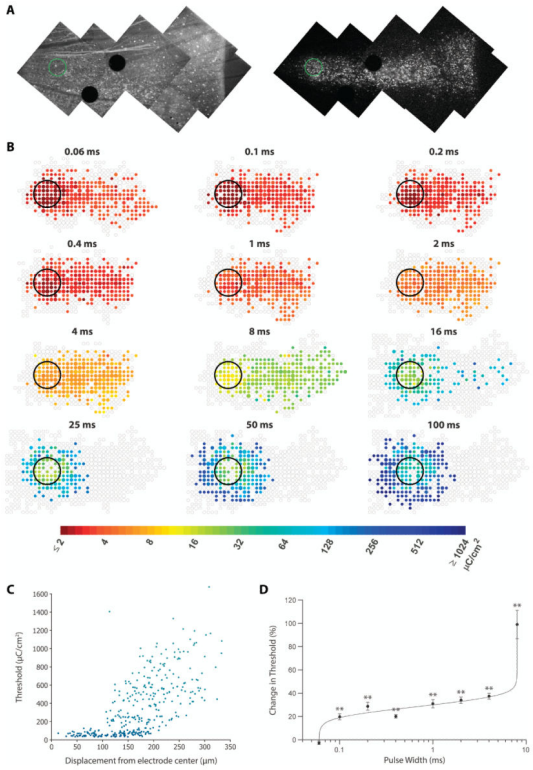

Fig. 1. Effects of stimulus pulse duration on RGC responses to electrical stimulation

Electrode size (200 μm diameter) is the same as the Argus II. (**A**) Burst stimulation with 0.4-ms pulses activated a streak of RGCs extending from the transparent stimulating electrode (green circle) to the edge of the retina. (Left) Fluorescence image mosaic of the GCaMP5G-labeled retina before stimulation. (Right) Background-subtracted GCaMP5G responses to electrical stimulation. (**B**) Spatial threshold maps. The stimulating electrode is drawn as a black circle. Each colored dot represents the average threshold charge density ($\log_2$ scale) needed to stimulate cells at its location. Unfilled gray dots indicate areas containing cells that did not respond to stimulation. Small, medium, and large dots specify 1–2, 3–4, and 5+ cells, respectively. Maps are oriented such that the optic disc lies to the left of the image, with axons running horizontally toward their originating somata on the right [same orientation as (A)]. Each map contains data from 3 or 4 retinas (table S2). (**C**) Threshold as a function of displacement from electrode center for 100-ms pulses (n = 344 RGCs). (**D**) Change in RGC stimulation threshold as a function of pulse width in the presence of synaptic blockers (CNQX, D-APV, L-APB, strychnine, and picrotoxin). Pulses longer than 8 ms did not evoke responses in the presence of blockers. Thresholds for all pulse widths except 0.06 ms rose significantly once blockers were applied (** indicates $P < 0.001$ compared to the no blocker condition with paired t-tests). Error bars indicate SEM. Data were fit with an inverse sigmoid: $y = -a \ln[b/(x - c) - 1] + d$.

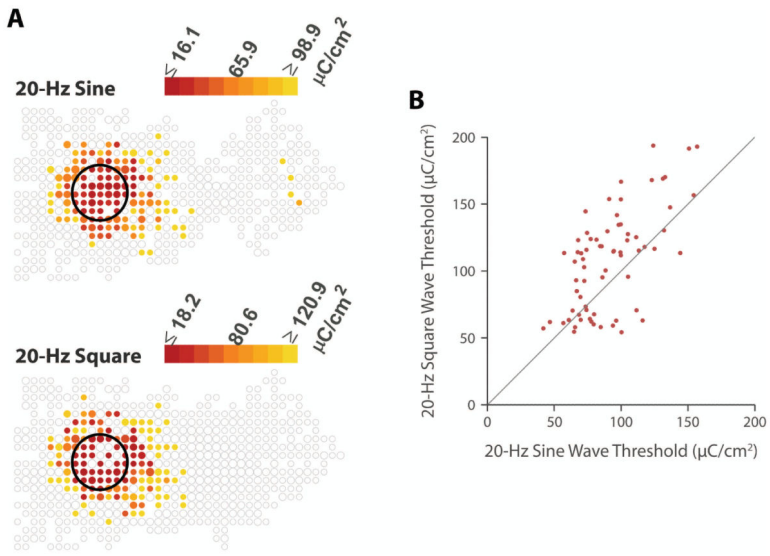

Fig. 2. Comparison of 20-Hz sine and square wave stimulation

Electrode diameter is 200 μm. Sine wave thresholds are specified in zero-to-peak amplitude. (**A**) Spatial threshold maps (as in Fig. 1B). The sine wave map (top) contains data from 3 retinas (table S2). Of the 344 cells that we imaged far (≥ 225 μm) to the right of the electrode perimeter, only 5 were stimulated antidromically. Based on the maximum stimulus amplitude delivered, minimum selectivity ratio (see Supplementary Materials) for 20-Hz sine waves was 16.7. The square wave map (bottom) is the same one shown in Fig. 1B for 25-ms pulses, except that the color scale has been changed. (**B**) Individual RGC thresholds for 20-Hz sine and square waves. Each data point represents a different cell (n = 121). Data were combined from two retinas. Square wave thresholds were 22.8 ± 35.5% higher than sine wave thresholds ($P < 0.001$, generalized estimating equations comparing means adjusted for repeated measures; percent change calculated from raw means).

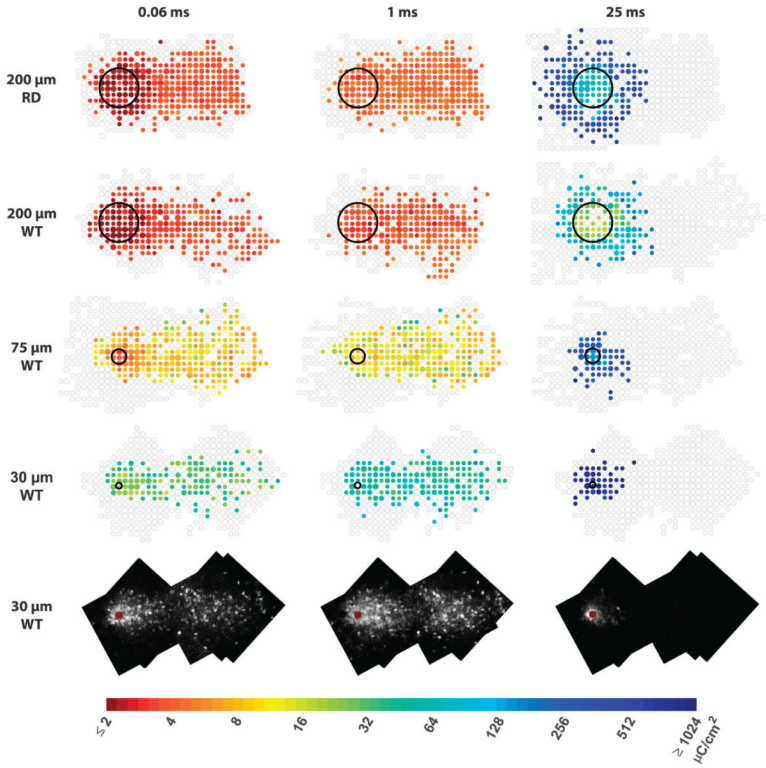

Fig. 3. Effects of retinal degeneration (top row) and electrode size (subsequent rows) on RGC responses to electrical stimulation

Spatial threshold maps for three pulse durations that cover the gamut of response types: direct RGC stimulation (0.06 ms, left column), combined ganglion and bipolar cell stimulation (1 ms, middle column), and bipolar cell stimulation (25 ms, right column) in RD and WT rats. Each map contains data from 3 or 4 retinas (table S2). In all cases, 0.06-ms pulses provided good selectivity for local somata over passing axons, 1-ms pulses provided poor selectivity (fig. S1), and 25-ms pulses produced focal responses. The bottom row shows background-subtracted GCaMP5G responses to suprathreshold stimuli for 30-µm-diameter electrodes (red circles). Images from each retina were transformed into the same reference frame and averaged.

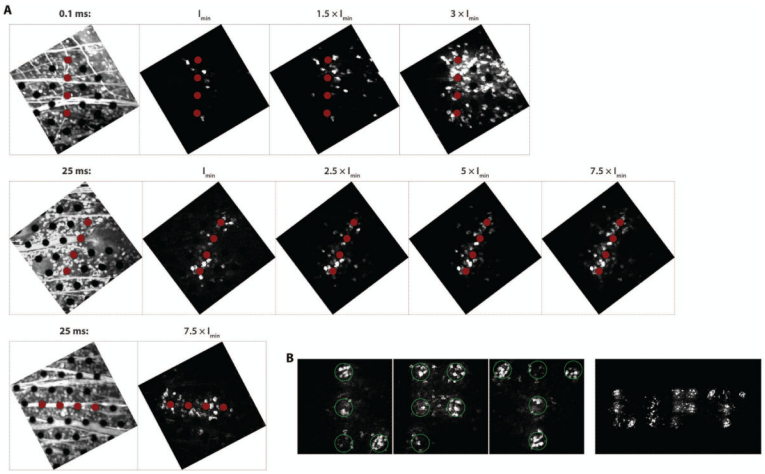

Fig. 4. Patterns resulting from multielectrode stimulation of RGCs

(**A**) Line stimulation with four 30-μm-diameter electrodes (red circles) on a 75-μm pitch. Electrodes are oriented transverse (top and middle rows) and parallel (bottom row) to axon bundles. Leftmost images show local ganglion cell layer anatomy as revealed by Alexa Fluor 594 fluorescence (see Materials and Methods). Subsequent images show background-subtracted GCaMP5G responses to stimulation at different amplitudes (I_{min} is slightly above threshold). Responses generally become stronger with increasing amplitude. (Top row) 0.1 ms pulse width. (Middle and bottom rows) 25 ms pulse width. (**B**) (Left) Letters patterned onto a single retina with transparent 75-μm-diameter electrodes (green circles) on a 150-μm pitch. Pulse width is 25 ms. The letters conform to the definition of Snellen optotype, which requires a critical detail size (stroke and gap width) that subtends 1/5 of the total height. (Right) The word *LIFT* spelled by combining the letters *L*, *F*, and *T* with a line pattern from (A). The image shows the actual size of the word at typical reading distance (40 cm).

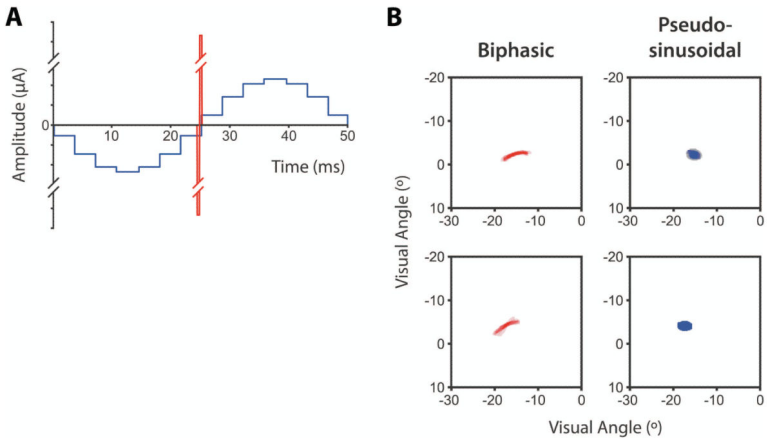

Fig. 5. Effect of stimulus pulse duration on phosphene shape in a retinal prosthesis subject

(**A**) The stimulus waveform, a train of either 0.45-ms/phase (red) or 25-ms/phase (blue) pulses, each applied at 20 Hz for a duration of 500 ms. Twenty-five millisecond pulses were presented as sinusoids in order to increase the likelihood of staying within electrochemical safety limits (see Fig. 2). Pseudo-sinusoids were used because the implant hardware does not permit stimulation with true sine waves. (**B**) Subject's drawings of phosphenes elicited from stimulation with electrode C4 (top row) and C3 (bottom row). Plots show the average percept drawn across up to 5 trials (see table S4). Electrode diameter is 520 μm (top row) or 260 μm (bottom row).